Materials Research Bulletin 171 (2024) 112607

Contents lists available at ScienceDirect

Materials Research Bulletin

journal homepage: www.elsevier.com/locate/matresbu

Research Papers

Study of the centers responsible for the TL emission by EPR and PL analysis of Eu-doped $CaSiO_3$ phosphors synthesized by the devitrification method

Carlos D. Gonzales-Lorenzo [a,b,*], T.K. Gundu Rao [a,**], Alberto A. Ccollque-Quispe [a], Jorge Ayala-Arenas [a], Monise B. Gomes [c], Betzabel N. Silva-Carrera [c], Roseli F. Gennari [b], Valeria S. Pachas [d], F. Monzon-Macedo [d], H. Loro [d], Jose F.D. Chubaci [b], Nilo F. Cano [e], René R. Rocca [e], Shigueo Watanabe [b]

[a] Universidad Nacional de San Agustín de Arequipa, Av. Independencia S/N, Arequipa, Peru
[b] Instituto de Física, Universidade de São Paulo, São Paulo, SP, Brazil
[c] Instituto de Pesquisas Energéticas e Nucleares, IPEN-CNEN/SP, Av. Prof. Lineu Prestes, 2242, Cidade Universitária, São Paulo, SP, Brazil
[d] Facultad de Ciencias, Universidad Nacional de Ingeniería, Lima, Peru
[e] Instituto do Mar, Universidade Federal de São Paulo, Santos, SP, Brazil

ARTICLE INFO

Keywords:
Eu doped $CaSiO_3$
Defects centers
PL
TL
EPR

ABSTRACT

$CaSiO_3$ doped at different ppm of Eu were synthesized by the devitrification method. Polycrystals exhibit a prominent high-temperature TL peak that increases in intensity and shifts toward higher temperatures with increasing amounts of dopant. TL emission spectrum of $CaSiO_3$: Eu displays two very broad bands centered at 400 and 440 nm corresponding to the temperatures of 229.5 and 373.5 °C, respectively. PL measurements indicate the presence of Eu^{2+} and Eu^{3+} ions. EPR spectrum arises from two defect centers. One of the centers with principal *g*-values 2.016, 2.0091, and 2.0051 is attributed to O^- ion and the center correlates with the TL peak at 236 °C. Center II with an isotropic *g*-value of 2.0018 is attributed to an F^+ center and the center relates to the TL peak at 120 °C. Center III is also tentatively identified as the F^+ center which is associated with the TL peak at 365 °C.

1. Introduction

Studies involving high-dose irradiation have been and are up to now of great interest in different research centers such as nuclear centers and industry due to its various applications such as sterilization of medical equipment, food preservation, and treatment of various materials. That is why a dosimetry system for the control of absorbed radiation must be carried out by different measurement techniques, including dosimetry by passive radiation detectors based on ionic crystals [1]. On the other hand, it is important to mention that silicate-based luminescent materials, either in their naturally occurring form or synthetically produced in a laboratory, have been the subject of interest for several years due to their diverse properties and uses. These materials present chemical and thermal stability [2–4], high sensitivity to ionizing radiation, low fading, and mechanical stability [5–10]. Among the silicates, we have tourmaline, aquamarine, lapis lazuli, quartz, calcium silicate, magnesium silicate, strontium silicate, and lithium silicate, among others. [5,7,10-12]. The advantage of synthetic silicates is that they can be manipulated and often doped with rare earth, transition metals, or any other element. This is, according to what is required by the researcher and for a specific purpose, either for its use as a detector of gamma radiation, protons, neutrons, and even heavy ions, etc. [6,7,9, 13]. In addition, these dopants within a silicate matrix can improve their luminescence and be used as a passive detector to be later taken and analyzed in the laboratory using different spectroscopic techniques such as Thermoluminescence (TL), Optically Stimulated Luminescence (OSL), Radioluminescence (RL), Photoluminescence (PL), Electron Paramagnetic Resonance (EPR), and Optical Absorption (OA), among others [14–16]. TL is the emission of light from a material when it is heated, and is used in radiation dosimetry applications, whilst EPR is a spectroscopic technique that detects unpaired electrons in a material, and is useful for studying the electronic properties of materials.

* Corresponding author at: Universidad Nacional de San Agustín de Arequipa, Av. Independencia S/N, Arequipa, Peru.
** Corresponding author.
E-mail addresses: cgonzaleslo@unsa.edu.pe (C.D. Gonzales-Lorenzo), tgundu@unsa.edu.pe (T.K. Gundu Rao).

https://doi.org/10.1016/j.materresbull.2023.112607
Received 18 June 2023; Received in revised form 24 October 2023; Accepted 6 November 2023
Available online 8 November 2023

Synthetic silicates used as matrices for various dopants have attracted the attention of many researchers, resulting in various studies that indicate silicates as one of the best host materials for rare earth ions [9, 17-24]. Among these, we have calcium silicate ($CaSiO_3$) and this material has been widely studied in recent years by several authors as an interesting host for Eu^{3+}, which shows remarkable luminescence spectra in the red region and with potential application in plasma technology [2, 4,6,25-27]. Additionally, it has been observed that when silicate-based materials are doped with Eu^{3+} and irradiated with ionizing radiation, these dopants can change their valence state by oxidation, reduction, or ionization processes, producing or creating defect centers such as F centers, centers of recombination, traps, absorption bands in the crystal structure [28,29]. Besides, Dai et al. [30] have shown that both Eu^{2+} and Eu^{3+} can coexist in the silicate phosphor of $Ba_{(1-x)}MgSiO_4$:xEu when synthesized under an air atmosphere. This is because the substitution of Eu^{3+} cations for Ba^{2+} cations triggers the formation of V_{Ba} vacancies that play the role of electron donors towards the Eu_{Ba} defects.

In a previous study, we prepared pure synthetic polycrystals of β-$CaSiO_3$ (pseudowollastonite) and a relation of the EPR centers responsible for the TL emission reported. This polymorph of $CaSiO_3$ shows O^- ion and F^+ defect centers in the lattice structure which behave like recombination centers in the TL process. These centers are responsible for the high-temperature TL peaks in β-$CaSiO_3$ [8]. The high-temperature TL peak at about 250 °C shows good stability, low fading, good reproducibility, and a dosimetric behavior when irradiated at a low gamma radiation dose, of the order of mGy to Gy. This behavior makes the study of the $CaSiO_3$ of great interest since higher temperature peaks are normally more stable at room temperature than lower temperature ones, and because it is possible to monitor the deposited gamma radiation through the intensity of the dosimetric and stable TL peak.

In this context, studies carried out by Katyayan et al. [12,31] have shown that the $CaSiO_3$ sample when doped with Eu presents three prominent TL peaks, standing out among them the highest temperature TL peak (at about 700 K at a constant heating rate of 5 °C/s), showing differences compared to the non-doped sample. This difference and the effect of the Eu dopants in the $CaSiO_3$ sample will be analyzed and studied in the present work in order to find the defects responsible for these differences in the TL response.

In this work, we will focus on calcium silicate due to its excellent luminescent properties. Properties such as TL, OSL, and PL of $CaSiO_3$, whether in its pure form, as well as doped with elements such as Eu, Tb, or Ce, have been reported and extensively studied [2,3,6-9,12,17,18,26, 27,32-35]. However, EPR studies of this doped material have not been found, and thus understand crystalline defects responsible for its luminescent properties.

2. Experimental details

2.1. Synthesis

In the production of the synthetic polycrystalline Eu-doped $CaSiO_3$, the devitrification method was employed [7,8]. 12.0 g (44.4 wt.%) of CaO (Anidrol-PA ACS, 99.9 %), 15.0 g (55.6 wt.%) of SiO_2, and an appropriate quantity of Eu_2O_3 (Sigma Aldrich/PA ACS, 99.99 %) were used to obtain an amount of 100, 550, and 1000 ppm of Eu as dopant in the CaO-SiO_2 mixture. All the initial reagents were placed in a pot with two alumina balls inside and sealed on the outside. The sealed pot was taken to a rotary mill for 8 h, thus obtaining a homogeneous mixture. Finally, the mixture with the dopant is then placed in an oven heated to 1500 °C to melt the above mixture, for two hours in an ambient atmosphere. The melt is then cooled slowly using a temperature controller so that the room temperature is reached after about 24 h. This polycrystalline sample of $CaSiO_3$ was crushed and sieved to retain grains 80–180 μm in size for TL and EPR measurements, while grains smaller than 0.080 mm in diameter were used in the structural analysis by X-ray diffraction (XRD) method. XRD data of powder sample at room temperature were obtained on Rigaku Miniflex 300 diffractometer with Cu $K_{\alpha 1}$ (0.15406 nm) radiation between 10° and 60° at a 0.02° (in 2θ) scanning step and a 1 s step time.

2.2. Gamma irradiation

Irradiations of Eu-doped $CaSiO_3$ samples (in powder form) for high doses in the region of hundreds of Gy up to 50 kGy were carried out at the Radiations Technology Center (CTR) of IPEN using Co-60 source type gamma-cell with a dose rate of 0.64 kGy/h. For ultra-high doses in the region of kGy and MGy (from 70 kGy to 0.9 MGy), samples were irradiated with a Co-60 gamma beam from the gamma-cell irradiator at the Nuclear Energy Department of the Federal University of Pernambuco (UFPE), Brazil, operating at 2.571 kGy/h (at the time of irradiation). Gamma irradiations at both institutions were performed at room temperature and under conditions of electronic equilibrium.

2.3. Luminescence measurements

TL measurements were carried out using Harshaw TL reader model 4500 in a nitrogen atmosphere; the heating rate was kept at 4 °C/s. Luminescence was detected by a Hamamatsu R647 photomultiplier tube through a Schott KG1 filter (transmission band 330–690 nm). Five TL reading measurements were carried out to obtain an average TL glow curve using a mass of about 1.8 mg of grain-shaped polycrystals (80–180 μm). All TL readings were carried out 24 h after the irradiation took place, time enough to reach the stability of the TL peaks in Eu-doped $CaSiO_3$ polycrystals.

TL emission spectrum was carried out with a RISØ TL/OSL DA-20 reader. Measurements were performed using different aliquots and a monochromator from 240 to 680 nm with a step of 20 nm.

Photoluminescence (PL) measurements were recorded at room temperature using Horiba Fluoromax-4 spectrofluorometer equipped with a 150 W CW Ozone-free xenon arc lamp. The light emission was detected by photomultiplier R928P, with spectral coverage between 200–870 nm.

2.4. EPR measurements

EPR measurements were performed at room temperature utilizing a MiniScope MS-5000 spectrometer from Freiberg Instruments. The EPR spectra were recorded at 9.45 GHz (X-band) microwave frequency, 20 mW microwave power, field modulation of 0.2 mT at 100 kHz, and a sweep time of 300 s. Additionally, a Bruker EMX spectrometer with a rectangular cavity (ST ER4102) with the same parameters was employed to compare EPR results. The *g*-factors of defect centers were calibrated using Diphenyl Picryl Hydrazyl (DPPH) as a standard sample.

3. Results

3.1. X-ray diffraction studies

The pseudowollastonite phase is a high-temperature polymorph of the $CaSiO_3$. This crystal structure has been studied by Yamanaka and Mori [36]. They have identified the presence of at least three polytype structures of β-$CaSiO_3$: four-layer, six-layer, and disordered stacking polytypes. First, the structure of the four-layer polytype is the dominant phase in their studies with a triclinic unit cell and solved in space group C1. Parameters of this structure were found to be: $Z = 24$, $a = 6.853$, $b = 11.895$, $c = 19.674$ Å, $\alpha = 90.12$, $\beta = 90.55$, $\gamma = 90.00°$. This structure consists of four Ca-octahedra layers and ternary rings of three tetrahedra of Si_3O_9 interposed between the layers. These Ca-octahedra in a layer are compressed in the c-direction, while tetrahedra of the rings are elongated in the same direction (stacking direction). Seryotkin et al. [37] have shown graphically the stacking sequence of layers for the

four-layer polytype structure with ternary rings of three tetrahedra in gray, Ca^{2+} ion in blue, and O^{2-} ion in red as shown in Fig. 1. The six-layer polytype has been indicated as having a pseudosymmetry C2/c and is probably isostructural with SrGeO3. Finally, the disordered structure was confirmed by diffuse streaks along c^* axis with the presence of many polytypes along c axis [36].

In the present work, XRD diffraction patterns were analyzed using the X'Pert HighScore Plus software [38] to identify the crystalline phases present in the samples. The diffractograms obtained are shown in Fig. 2. For all samples, the diffraction peaks correspond mainly to diffraction patterns of different phases such as $CaSiO_3$ and SiO_2. For the case of $CaSiO_3$ doped with Eu at 100 and 550 ppm, similar diffraction patterns are shown. All the diffraction peaks in the spectrum are coincident with the calcium silicate (pseudo-wollastonite $CaSiO_3$), and 2 types of silicon oxide (Cristobalite low and Quartz Alpha - SiO_2) matched with 01-089-6463, 01-077-1317, and 01-089-8937 PDF-2 files, respectively. Similarly, for the case of $CaSiO_3$ doped with Eu at 1000 ppm, all the diffraction peaks in the spectrum are coincident with the calcium silicate (pseudo-wollastonite $CaSiO_3$), and 2 types of silicon oxide (tridymite and Cristobalite – SiO_2) matched with 01-074-0874, 96-810-4535, and 96-900-1580 PDF-2 files. Calculated semi-quantitative phase percentages using the X'Pert HighScore Plus software have shown that, for all cases, about 85 % of the sample belongs to pseudo-wollastonite and 15 % to silicon oxide. β-$CaSiO_3$ type polycrystalline structure is observed to dominate in this sample. The pseudo-wollastonite phase found for the Eu-doped $CaSiO_3$ at 1000 ppm corresponds to the same crystal structure found by Yamanaka and Mori [36] with the same crystal data, and whose four-layer polytype structure of $CaSiO_3$ is shown in Fig. 1. It is worth noting that the final formation of the polycrystalline compound using the devitrification method depends on the appearance of seeds within the liquid which depends largely on the shape of the crucible that contains the substance or on some impurity within the compound that breaks the homogeneity of the compound.

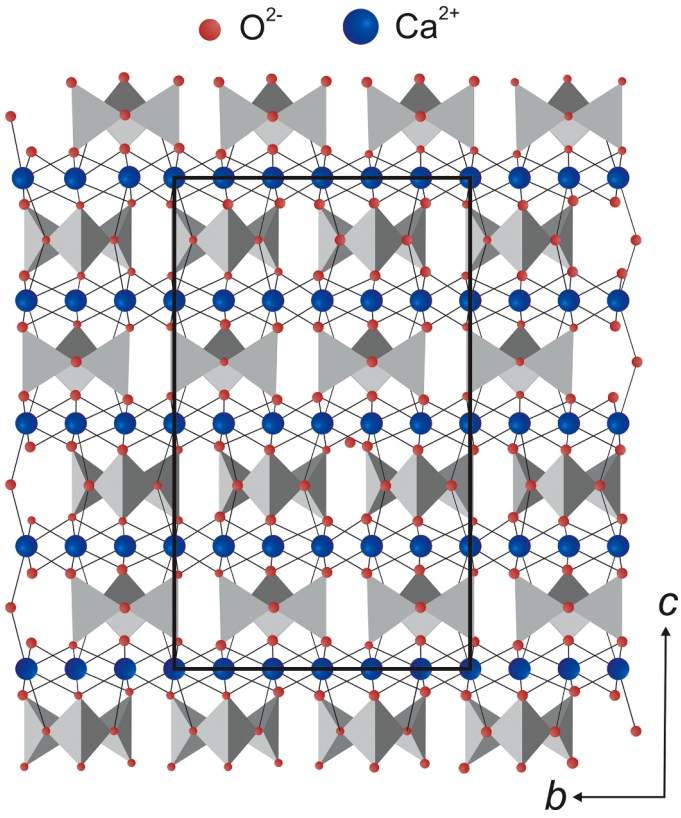

Fig. 1. Stacking sequence of layers of (Si_3O_9) rings in four-layer pseudo-wollastonite polytype. After [37].

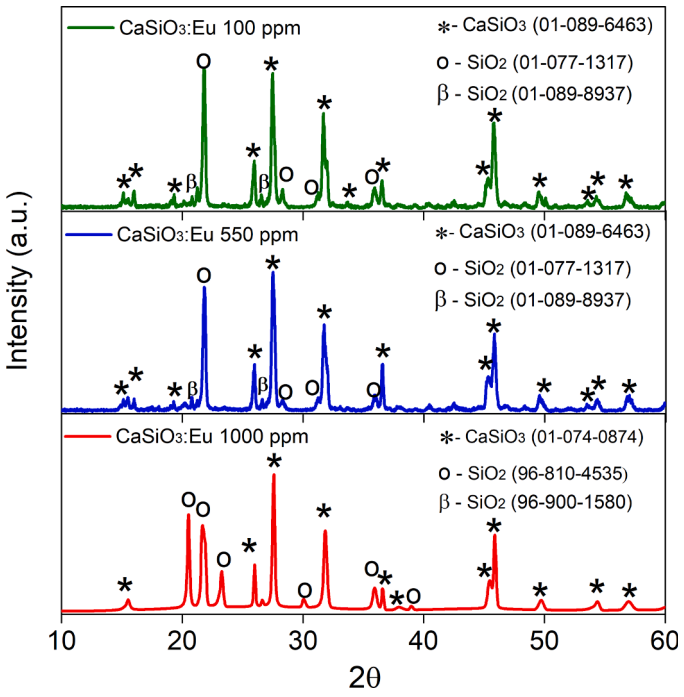

Fig. 2. XRD patterns of $CaSiO_3$ doped with Eu at 100, 550, and 1000 ppm. (*) belongs to $CaSiO_3$; (o) and (β) corresponds to the different polymorphs of SiO_2. The match PDF-2 files to the diffraction patterns using the X'Pert HighScore program are shown.

Both samples doped with 100 and 550 ppm of Eu present a similar crystalline structure, which indicates that the dopant has the same influence on the crystalline formation of the compounds (Fig. 2). On the other hand, the same sample doped with Eu 1000 ppm, presents different phases to those mentioned before. This is because, amounts of doping greater than 1000 ppm can influence the formation of the crystalline structure which may be acting as a greater number of starting points (seed points), especially in a process of high temperature and instability. This influence is seen not in the change of the compounds itself from $CaSiO_3$, and SiO_2, but rather in the formation of different phase types of the same compounds as can be seen in Fig. 2.

3.2. Luminescence studies

The Eu-doped $CaSiO_3$ samples were irradiated with a gamma dose of 30 kGy dose from a Co-60 source. TL glow curves of irradiated samples are shown in Fig. 3. As can be seen in this figure, the sample of $CaSiO_3$ doped with 100 ppm of Eu exhibits two TL peaks at approximately 208 and the prominent peak at 340 °C. For the case of $CaSiO_3$ doped with Eu with 550 ppm, TL glow curves show peaks at about 260 and a prominent peak at 338 °C. Finally, for the case of $CaSiO_3$ doped with Eu at 1000 ppm, TL glow curves display peaks at about 120 °C, 236 °C, and a prominent TL peak at 365 °C. Among the samples prepared in this work, the TL glow curve for the case of 1000 ppm of Eu shows more intense TL peaks with better clarity which can be more easily identified compared to the other two doped samples.

TL glow curves shown in Fig. 3 are composed of several TL individual peaks as can be seen in the GDC process as shown in Fig. 6(b). In particular, the highest temperature TL peak is mainly composed of three individual peaks and the most prominent is the highest temperature individual TL peak at about 383 °C. This individual peak appears to be highly dependent on the concentration of the Eu dopant. Therefore, for increasing ppm amount of Eu dopant, this individual TL peak shows a higher TL intensity, thus showing a greater intensity in the corresponding experimental TL peak. This process gives the effect of

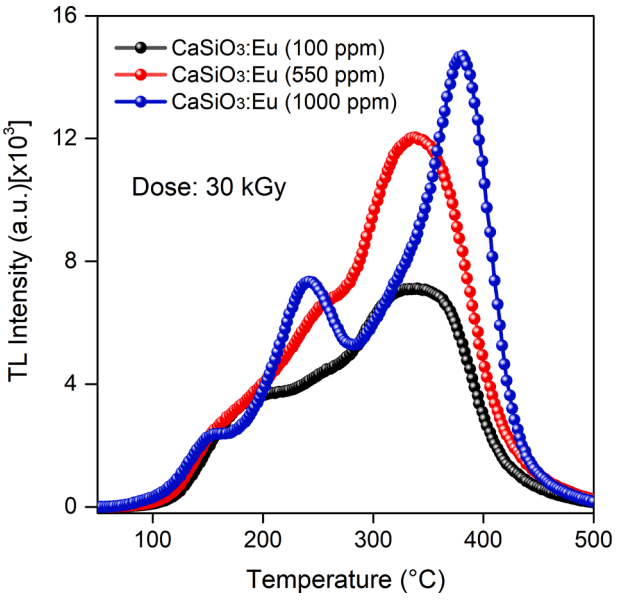

Fig. 3. TL glow curves of $CaSiO_3$ doped with 100, 550, and 1000 ppm irradiated with a gamma dose of 30 kGy from a Co-60 source. The heating rate was kept at 4 °C/s, and a mass of about 1.8 mg was used for each measurement.

displacement towards the right side of the experimental high-temperature TL peak when irradiated to a high gamma radiation dose (50–900 kGy).

$CaSiO_3$ doped with 1000 pm Eu was irradiated at different doses of gamma radiation from 500 Gy to 900 kGy to study the dose dependence as its thermoluminescence is concerned. Fig. 4(a) shows the TL curves of the mentioned sample irradiated from 500 Gy to 50 kGy while Fig 4(b) shows the TL curves for gamma radiation doses from 70 to 900 kGy. It is important to note here that the TL peaks shown for the Eu-doped $CaSiO_3$ sample differ from our previous studies for the undoped $CaSiO_3$ sample [7–9]. For the undoped sample of $CaSiO_3$ irradiated at high doses (above 500 Gy), three peaks around 124, 250, and 306 °C are observed. The second peak around 250 °C is the prominent peak, visibly standing out from the other two, reaching its saturation for a dose of 3 kGy. It can be seen that the Eu-doped sample converts the third TL peak around 365 °C into the prominent peak compared to the undoped sample. In this work with the EPR analysis, we will try to reveal which defects could be contributing to the decrease in the TL intensity of the second peak and the predominance of the third TL peak. The behavior of this prominent third peak has also been previously reported by Katyayan et al. [12,31].

Fig. 5(a) and (b) show the TL response of the two main TL peaks for doses ranging from 500 Gy to 900 kGy for TL peaks at 236 °C and 365 °C, respectively. Analyzing the dose-response curves with log axes on the same scale, the TL peak at 236 °C shows an increasing behavior from 500 Gy to 15 kGy. From this point, the TL peak at 236 °C shows saturation at 15 kGy followed by a linear decrease in the logarithmic scale with the increase in dose. A linear fitting within the dose range between 15 and 900 kGy can be expressed as log (TL) = −0.243*log (dose) + 5.030. In that sense, this second experimental TL peak presents promising characteristics for its use in high radiation dosimetry (kGy - MGy). On the other hand, Fig. 5(b) shows an increasing non-linear behavior of the TL peak at 365 °C from 500 Gy to 30 kGy reaching its saturation point. After that, the dose dependence of the TL peak at 365 °C shows a second growth curve which reaches a second saturation for a dose of 500 kGy and then has a decrease in TL intensity with the dose.

It is seen that the TL curve of the Eu-doped $CaSiO_3$ sample with 1000 ppm Eu presents TL peaks that can be identified and studied in more detail. In order to find the number and position as well as the activation energy of the TL peaks contained in the complex experimental glow curve of the phosphor, the T_M-T_{stop}, $E-T_{stop}$, initial rise method, and

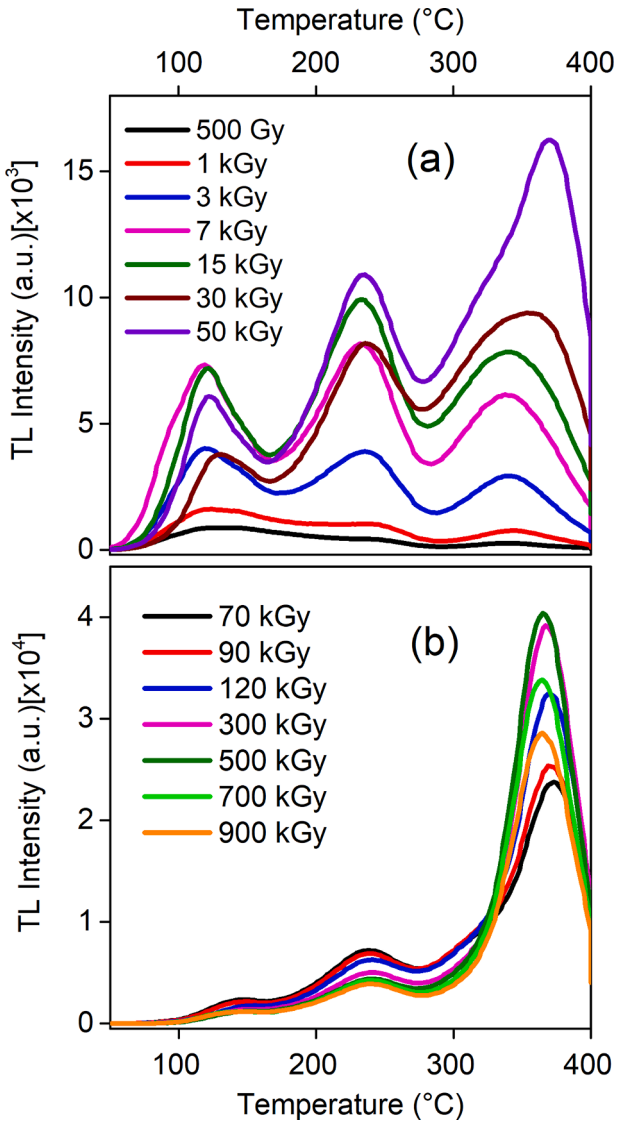

Fig. 4. TL glow curves of $CaSiO_3$ doped with 1000 ppm of Eu irradiated with low gamma doses of 500 Gy up to 50 kGy, and (b) of 70 up to 900 kGy. A heating rate was kept at 4 C/s, and a mass of about 1.8 mg was used for each measurement.

glow-curve deconvolution methods were used [39–41].

The initial rise method is based on the fact that the initial part of the TL glow curve can be described by exponential behavior as $\exp(-E/kT)$. To obtain reliable results, points below 15 % of the maximum TL intensity should be considered [40]. Subsequently, using the Arrhenius diagram: $\ln(I_{TL})$ vs $1/T$ which will be approximated as a straight line, the activation energy E can be easily obtained from the slope $-E/k$. For the $E-T_{stop}$ method, the activation energy was found using different pre-heating temperatures (T_{stop}) from 55 to 400 °C at a 5 °C scanning step. For each T_{stop}, the TL glow curve was recorded and its corresponding activation energy was calculated. Obtained activation energies (E) using the $E-T_{stop}$ method for the Eu-doped $CaSiO_3$ sample are shown in Fig. 6(a). In this figure, we can distinguish seven possible activation energies that accumulate in the form of increasing horizontal segments. This in turn indicates the number of individual TL glow curves present in the experimental TL glow curve of the Eu-doped $CaSiO_3$ sample.

As an important complement, the glow-curve deconvolution (GCD) method is also used in several studies to compute characteristic parameters like E, s and the order of the kinetic (b) of individual glow peaks on the experimental TL glow curve [42].

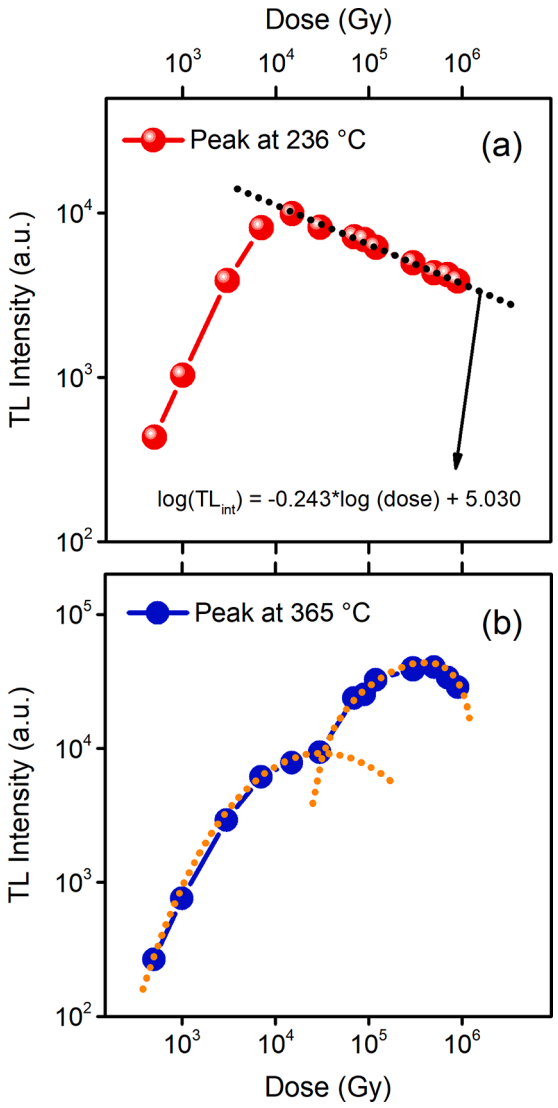

Fig. 5. (a) TL glow curves of $CaSiO_3$: Eu (1000 ppm) irradiated with gamma dose of 0.5–900 kGy. (b) T intensity vs. dose-response using a mass of about 1.8 mg.

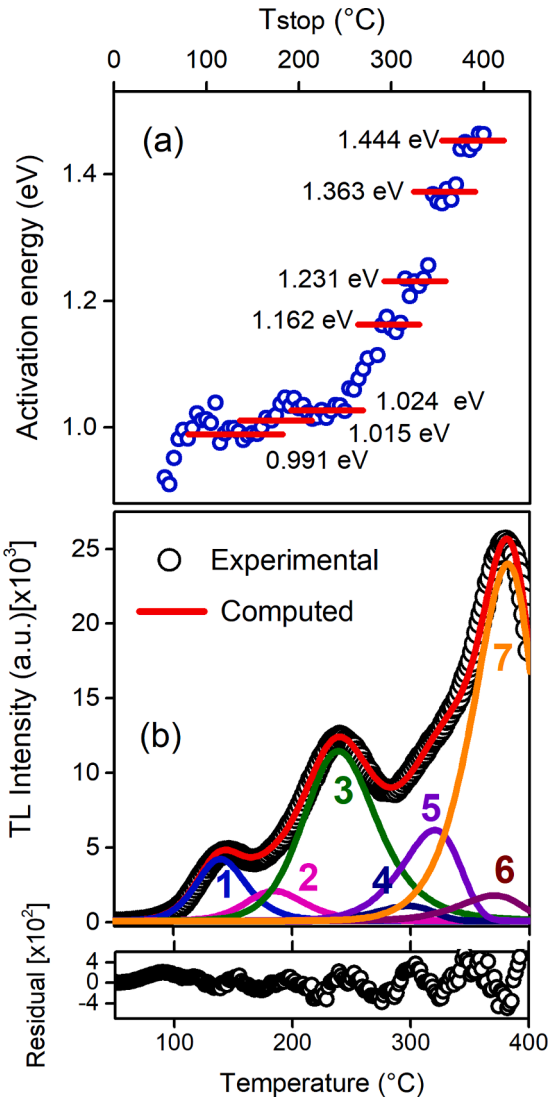

Fig. 6. (a) Activation energy vs. Tstop method. (b) TL glow curve of $CaSiO_3$ doped with 1000 ppm of Eu irradiated with gamma dose of 50 kGy from 60-Co source. A good fit between the experimental glow curve (circles) and the simulated glow curve (red line) can be achieved by assuming the presence of seven peaks.(For interpretation of the references to color in this figure legend, the reader is referred to the web version of this article.)

The position of the first and second experimental TL peaks at about 120 and 236 °C peak shift to lower temperatures with increasing doses as shown in Fig. 4. Thus, a second-order peak will be more appropriate for these peaks. For the third peak, however, the position at about 365 °C seems to be the same with increasing doses. Hence, a first-order peak will be more appropriate. Using the previous results found by the $E-T_{stop}$ method, the position of the possible TL peak by the T_M-T_{stop} results, and applying the equation proposed by Kitis et al. [42] we obtain the deconvolution of the TL glow curve of the phosphor that has been irradiated with a gamma dose of 50 kGy (see Fig. 6b). The measurements carried out for the deconvolution analysis were carried out several days after its irradiation to avoid the fading effect, especially in the high-temperature TL peaks around 236 °C and 365 °C which are of greatest interest for dosimetry purposes. The TL glow curves in Fig. 4 present three well-defined peaks and the GCD method shows seven overlapping TL peaks. Fig. 6(b) shows these computed TL peaks separated using different orders of kinetics at about 140, 185, 239, 298 320, 370, and 383 °C. Quality of fit was tested with the Figure of Merit (FOM) [43]. FOM = 1.07 % shows that the data fit is satisfactory. Fig. 6(a) shows the obtained activation energies (E) using the $E-T_{stop}$ method. The position, activation energies (E), and frequency factor (s) of TL peaks of the Eu-doped $CaSiO_3$ (1000 ppm) sample are shown in Table 1.

Table 1
Kinetic order, TL peak position, activation energy (E), frequency factor (s) of TL peaks of Eu doped $CaSiO_3$ calculated by GCD. FOM = 1.07 %.

Peak	Kinetic order	TL peak (°C)	E (eV)	s (s^{-1})	τ (years at 25 °C)
1	2nd	140	0.991	3.31×10^{11}	0.005
2	2nd	185	1.015	3.28×10^{10}	0.139
3	2nd	239	1.024	2.16×10^{9}	2.99
4	1st	298	1.162	2.96×10^{9}	469
5	1st	320	1.231	4.68×10^{9}	4.36×10^{3}
6	1st	370	1.363	7.33×10^{9}	4.74×10^{5}
7	1st	381	1.444	2.09×10^{10}	3.89×10^{6}

Fading studies of Eu-doped $CaSiO_3$ have shown the same fading as the undoped polycrystalline $CaSiO_3$ produced previously [8,9]. After 48 h, TL peaks of the Eu-doped samples exhibit no decay.

The TL emission spectrum of the polycrystalline Eu-doped $CaSiO_3$ presented two very broad bands centered at 400 and 440 nm corresponding to the temperatures of 229.5 and 373.5 °C, respectively, as

observed in Fig. 7. Furthermore, this spectrum shows two low-intensity peaks centered at 440 and 600 nm that corresponds to the temperature of 153 and 238.5 °C, respectively. Low-temperature TL peaks do not appear because they must have decayed by the time that has passed since irradiation and reading measurements. Thus, the majority of contribution comes from photons with wavelengths between 400 and 440 nm, which represent the TL peaks around 153, 229.5, and 373.5 °C and photons of wavelengths between 580 and 600 nm contribute to the low-intensity TL peak around 238.5 °C.

As seen above, the TL peak for the $CaSiO_3$ samples doped with Eu at 1000 ppm and irradiated at 50 kGy gamma dose (as shown in Fig. 3) shows three TL peaks around 122, 236, and 369 °C. The small discrepancies found in the TL peaks in the emission spectrum in Fig. 7 and the TL curve in Fig. 3, arise from using two different instruments viz., the RISØ TL/OSL DA-20 reader and Harshaw 3500 equipment, respectively.

Usually, Eu^{3+} ions display an orange-red or red emission which is produced by the $^5D_0$-^7F_J (J = 0–4) transition, whilst Eu^{2+} ions show strong and broad blue, blue-green, or green emission produced by the $4f^65d^1$-$4f^7$ transition (350–560 nm) [44,45]. It is important to mention that Eu displays different luminescence characteristics according to its valence. Eu^{3+} exhibits a red-light emission, while Eu^{2+} according to the host may emit anywhere from UV to the deep red region (250–400 nm) [25,45]. In the present work for the TL process, the presence of Eu^{2+} ion is evident since wavelengths between 400 and 440 nm are shown in the TL spectra (Fig. 7). It is important to mention that, the second peak at about 236 °C, although its emission corresponds to 400 nm as shown in Fig. 7, it would not depend entirely on the same process of emission from Eu^{2+} ion. In this case, the O- ion center could be related to this TL peak as will be explained in the next section. Furthermore, this peak is also observed in the undoped $CaSiO_3$ as shown in our previous research work [8]. In this sense, the contribution of the emission of Eu^{2+} ions could contribute mainly to the highest temperature peak at 356 °C. In addition, TL spectra show a low-intensity peak centered at 600 nm which could correspond to the presence of Eu^{3+} ions. In this sense, PL measurements were carried out to demonstrate the presence of both Eu^{2+} and Eu^{3+} ions.

Fig. 8 shows the PL emission spectra in the broad wavelength region

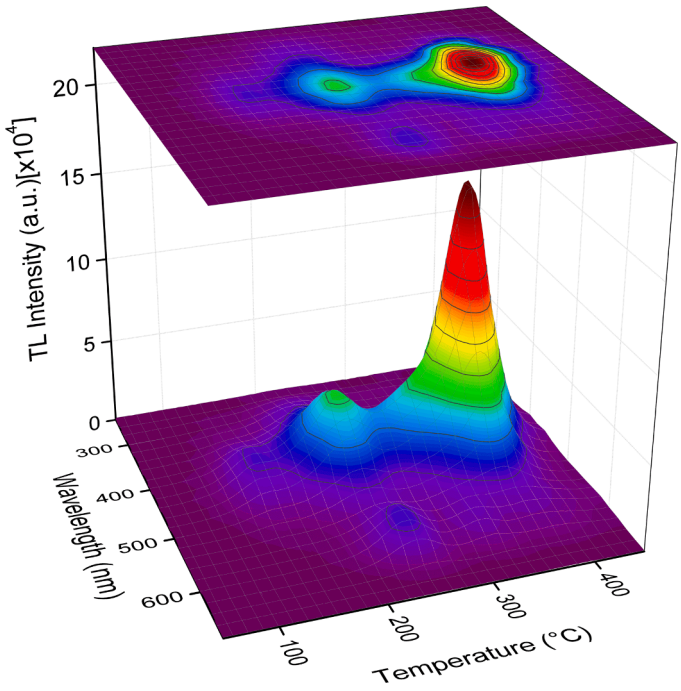

Fig. 7. TL spectra of Eu-doped $CaSiO_3$ (1000 ppm) sample after gamma irradiation dose of 50 kGy from a Co-60 source.

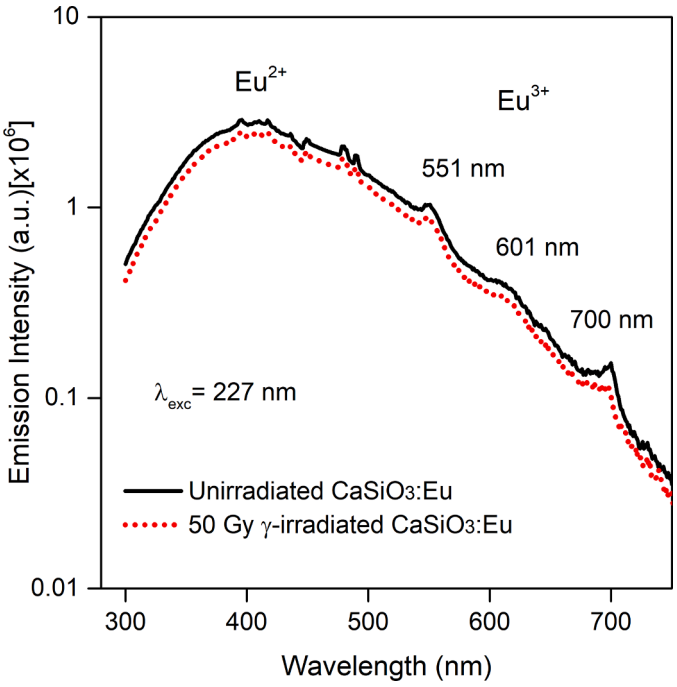

Fig. 8. PL emission spectra of polycrystalline $CaSiO_3$: Eu for excitation wavelength 227 nm. The solid line is for the non-irradiated sample and the dotted line is for the sample irradiated with 50 Gy of gamma dose.

at the range of 300–750 nm of non-irradiated and 50 Gy gamma-irradiation (from Co-60 source) of $CaSiO_3$: Eu (1000 ppm) monitored at the wavelength excitation of 227 nm ([6]). The axis corresponding to the PL intensity is shown on a logarithmic scale to visualize the PL peaks corresponding to the Eu^{3+} ion. In this figure, the broad band between 300 and 550 nm corresponds to the presence of Eu^{2+} ions whereas the peaks at 551, 601, and 700 nm could correspond to the emission bands from the $^4f_6$ electronic configuration of Eu^{3+} ions. It can be observed that the irradiated sample shows a decreasing intensity of about 18 %, concerning the PL intensity of the non-irradiated sample, especially in the band corresponding to the presence of the Eu^{2+} ion. Besides, in Fig. 8 is possible to observe that PL emission in the Eu^{2+} band (330 and 550 nm) results in the higher luminescence intensity of Eu^{2+} ions while Eu^{3+} ions luminescence is negligible. Consequently, it is possible to mention that the sample produced by the devitrification method at a temperature of 1500 °C under ambient conditions presents both Eu^{2+} ions as well as Eu^{3+} ions, although the latter is in low concentrations, as previously predicted. Other authors have reported that Eu^{3+} ions could be reduced to Eu^{2+} (reduction process) and at the same time oxidation process ($Eu^{2+} \rightarrow Eu^{3+}$) by initial gamma irradiation at room temperature [46, 47]. However, after the results shown in Fig. 8, it can not be concluded that these reduction or oxidation processes are occurring in the Eu-doped $CaSiO_3$ matrix. PL measurements of silicate-based samples doped with Eu and irradiated at high radiation doses of the order of kGy are being carried out. These results will be presented in future research reports.

3.3. EPR measurements

The room temperature Electron paramagnetic resonance (EPR) spectrum of gamma irradiated (dose: 30 kGy) $CaSiO_3$: Eu phosphor is displayed in Fig. 9. Based on thermal annealing studies, it could be inferred that two defect centers contribute to the observed spectrum. The two defect centers are labeled in Fig. 9. Center I is characterized by a rhombic g-tensor with principal values 2.016, 2.0091, and 2.0051. The linewidth of the central line (g = 2.0091) is about 11 gauss.

Calcium metasilicate, $CaSiO_3$, is known as Wollastonite and exists in

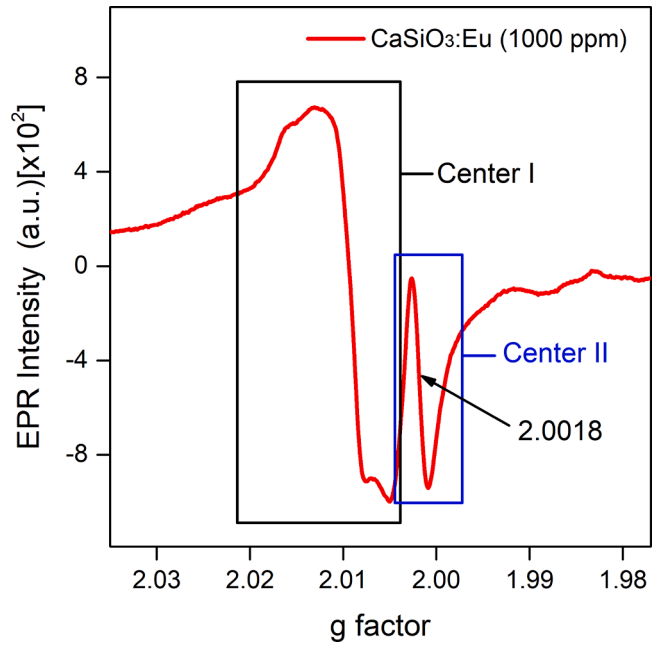

Fig. 9. EPR spectrum of Eu doped $CaSiO_3$: Eu phosphor irradiated with 30 kGy gamma dose from a Co-60 source.

two structurally different forms. The high-temperature form called pseudo-wollastonite (β-$CaSiO_3$) crystallizes in the triclinic form. The low-temperature form has two structural modifications, viz., wollastonite-2M and wollastonite-T_c. Wollastonite-2M crystallizes in monoclinic symmetry while the wollastonite-T_c has triclinic symmetry. Wollastonite-M has a perovskite structure with space group $P_{2/c}$. The structure has been refined by Hesse [48] and it was observed that three bridging oxygens connect the Si tetrahedron. Six non-bonding oxygen connect only to one Si. Wollastonite-2M has a chain silicate structure and the repeat unit contains three (SiO_4) tetrahedra. Oxygen atoms coordinate the Ca atom and form an approximate octahedron. Ca^{2+} ion in CASO (Ca—Si—O) lattice is in octahedral coordination and the ionic radius of Ca^{2+} ion in a sixfold coordination is 1.0 Å [49]. Si^{4+} ion has an ionic radius of 0.26 Å in fourfold coordination. Eu^{3+} ion has an ionic radius of 0.947 Å in sixfold coordination whilst Eu^{2+} ion has an ionic radius of 1.17 Å in sixfold coordination. As the ionic radius of Eu^{3+}/Eu^{2+} ion is close to that of Ca^{2+} ion as compared to Si^{4+}; Eu^{3+} or Eu^{2+} ion most likely substitutes Ca^{2+} ion in CASO lattice as shown in Fig. 10.

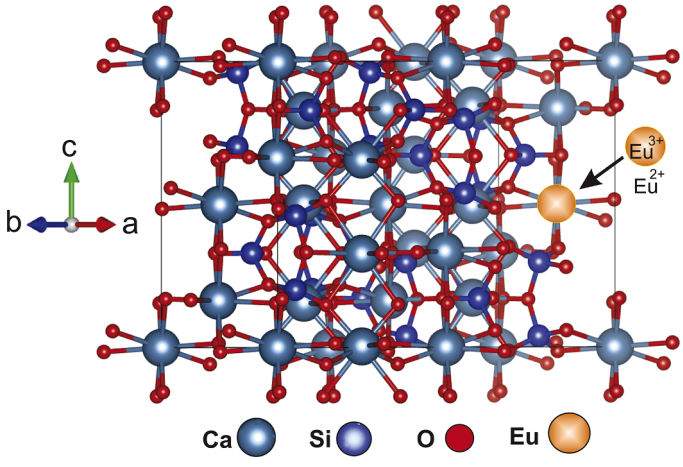

Fig. 10. Substitution of the Ca^{2+} ion by the Eu^{3+} or Eu^{2+} ion in the $CaSiO_3$ lattice. The crystal structure of $CaSiO_3$ was obtained from the 9011222.CIF file of the COD database.

The crystal structure of $CaSiO_3$ was obtained from the 9011222.CIF file of the Crystallography Open Database (COD) which is based on the studies of Yamanaka and Mori [36].

Oxide systems in general, after γ-irradiation exhibit F^+ centers, F centers, and O^- ions (V centers). γ-irradiation also produces oxygen ion vacancies through the displacement of oxygens to interstitial sites. The anion vacancy thus formed can trap electrons to form F^+ centers. On the other hand, interstitial oxygens can trap holes to form O^- ions. In an earlier study on an oxide system, BeO, Herve and Maffeo [50] observed after electron beam irradiation a single absorption line with an isotropic *g*-value of 2.0117. The line was attributed to an O^- ion. The support to this assignment of center in electron irradiated BeO single crystal is provided by correlation with a previous study [51] on the same BeO single crystal which was gamma irradiated at room temperature. O^- ion, in general, is characterized by an axial *g*-tensor with the perpendicular component greater than g_e (2.0023) while the parallel component will be nearly equal to g_e. An example is the O^- ion in Magnesium Oxide [52]. O^- ion also displays a rhombic *g*-tensor in some lattices. In a study on anatase nanoparticles, Misra et al. [53] observed the ion to have a rhombic *g*-tensor with principal values, $g_x = 2.0$, $g_y = 2.01$, and $g_z = 2.03$. There are also oxide systems where an isotropic *g*-value is observed for the O^- ion as in the BeO system. An example is the study on $MgAl_2O_4$ by Ibarra et al. [54]. After X-irradiation, $MgAl_2O_4$ shows a center with similar features as the center I. The *g*-value is 2.011 and an optical absorption band is observed at about 3.4 eV. Based on the optical absorption spectra, it was concluded that the center responsible for the EPR spectra and the associated absorption band is a hole-trapped oxygen ion i.e., a V-type center. Based on the previous studies mentioned above and consideration of centers that are likely to be formed in $CaSiO_3$, center I in $CaSiO_3$ is tentatively assigned to an O^- ion. The observed positive *g*-shifts of center I are also in accordance with the expectations of an O^- ion. The stability of center I was measured using the pulse-thermal annealing method. After heating the sample to a given temperature, it was maintained at that temperature for three minutes. Later it was cooled to room temperature for EPR measurements. Fig. 11 shows the thermal annealing behavior of center I. It is observed that the center becomes unstable at about 120 °C and decays in the temperature region 120–280 °C. This decay indicates that center I has the possibility of relating to the TL peak at 236 °C. Gamma irradiation can induce the formation of an F^+ center (an electron trapped at an anion vacancy) in

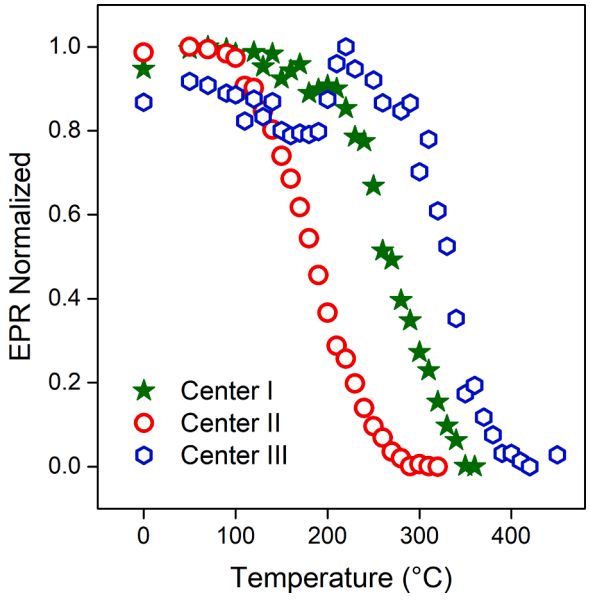

Fig. 11. Thermal annealing behavior of Center I (O^- ion), Center II (F^+ center), and Center III (F^+ center) in $CaSiO_3$: Eu phosphor. The intensity was normalized by the maximum value of the EPR signal for each center.

an oxide system like CASO. In the first EPR observation in an alkali halide, F^+ center displayed a relatively large linewidth of about 100 gauss [55]. However, the inherent linewidth of the center is small and is about 1 gauss [56]. The observed linewidth is decided by the amount of delocalization of the unpaired spin and its interaction with the neighboring ions. The observed linewidth also depends on the relative abundance of the isotopes of the neighboring ions and their respective magnetic moments. In alkali halides, where large line widths are generally observed, there is considerable delocalization of the unpaired electron that results in interaction not only with the immediate neighbors but also with alkali and halide ions in successive neighboring shells. For example, in LiCl and KCl, linewidths of 58 gauss and 20 gauss are respectively observed [57]. Irradiation causes an anion vacancy to capture an electron resulting in the formation of an F^+ center. The center displays positive and also, negative *g*-shifts, and the observed *g*-values are found to be close to the free-spin value (2.0023). In CASO: Eu phosphor, center II has a *g*-value equal to 2.0018 and the *g*-shift is relatively small. The linewidth is small and is about 2 gauss. Based on the known features of the F^+ center, center II is tentatively assigned to an F^+ center. As mentioned earlier, oxygen vacancies are present in CASO lattice and these vacancies trap electrons forming F^+ center. Fig. 11 shows also the thermal annealing behavior of center II. Center II becomes unstable at about 90 °C and decays in the temperature range of 90–290 °C. Hence, it is speculated that center II may be associated with the low TL peak at 120 °C.

Experiments have been carried out to observe the effect of increasing dopant ion concentration on the EPR spectrum. Fig. 12 displays the EPR spectra for Eu^{3+} ion concentrations ranging from 100 ppm to 1000 ppm. It is seen that apart from centers I and II observed in the phosphor with high Eu^{3+} ion concentration, an additional EPR line (center III) is observed at a *g*-value equal to 2.0004 in the phosphor with low dopant concentration (100 ppm, 550 ppm, and 750 ppm). The linewidth of the line is about 4 gauss. Center III line is not clearly seen at high dopant concentration as the center I and II lines dominate the spectrum. Based on the reasons mentioned earlier for the center II assignment, center III is also tentatively identified as an F^+ center. The result of the thermal annealing of center III is displayed in Fig. 11. It is seen that the center is unstable at around 240 °C and decays in the temperature range of 240 to 420 °C. It appears that this center is associated with the TL peak at 365 °C.

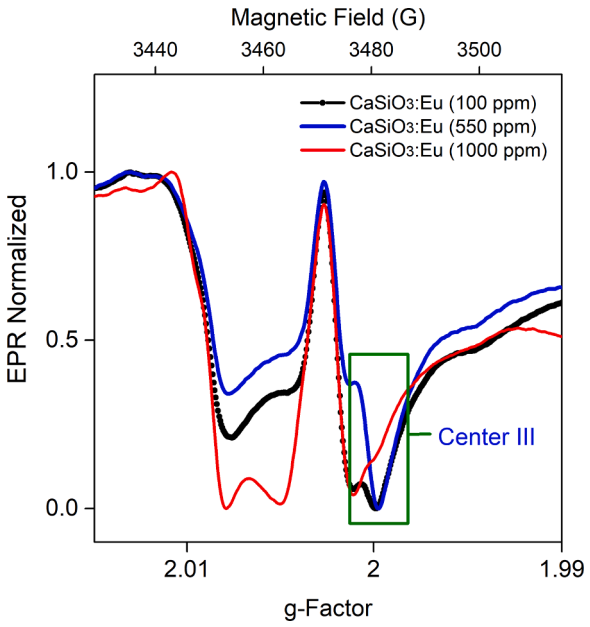

Fig. 12. EPR spectrum of $CaSiO_3$: Eu phosphor with different concentrations of the Eu^{3+} ion.

4. Conclusions

$CaSiO_3$ doped with 100, 550, and 1000 ppm of Eu has been synthesized by the devitrification method and the XRD pattern displays a main phase identified as pseudowollastonite (β-$CaSiO_3$) accompanied by a minor phase composed of two types of silicon oxide (tridymite and Cristobalite – SiO_2).

With increasing amounts of Eu dopant, the highest temperature TL peak shows a higher TL intensity. As a consequence, TL glow curves give the effect of displacement towards the right side of the experimental high-temperature TL peak when irradiated to a high gamma-radiation dose (50–900 kGy).

$CaSiO_3$: Eu (1000 ppm) exhibits TL peaks at 120 °C, 236 °C, and a prominent TL peak at 365 °C. This material shows a range dosimetric capability to very high gamma radiation dose within the dose range between 15 and 900 kGy for the TL peak at 236 °C. The best fit between the experimental TL glow curve and the simulated TL glow curve is found with seven computed TL peaks, the first three being of second order and the last four of the first order. Tm-Tstop, GCD, and initial rise technique were the methods used in this fit.

According to the TL emission spectrum for the $CaSiO_3$: Eu (1000 ppm) phosphor, the largest contribution of the TL response comes from photons with wavelengths of 400 and 440 nm corresponding to the temperatures of 229.5 and 373.5 °C, respectively. In addition, photons between 580 and 600 nm wavelength contribute to the low-intensity TL peak around 238.5 °C. The prominent highest temperature TL peak appears for high gamma-radiation in Eu-doped $CaSiO_3$ where the appearance of Eu^{2+} is mainly responsible for the 440 nm photon emission and Eu^{3+} ions for the photon emission at 600 nm. The PL measurements of the $CaSiO_3$: Eu samples before and after gamma irradiation show the presence of Eu^{2+} and Eu^{3+} ions. These results confirm the emission of the two types of Eu ions in the TL spectrum.

Three defect centers have been identified in the gamma-irradiated $CaSiO_3$: Eu phosphor. These are tentatively assigned to O^- ion, and F^+ centers. O^- ion is observed to correlate with the 236 °C TL peak while one of the F^+ centers (center II) relates to the TL peak at 120 °C. The other F^+ center (center III) is associated with the TL peak at 365 °C.

CRediT authorship contribution statement

Carlos D. Gonzales-Lorenzo: Writing – original draft, Methodology, Investigation. **T.K. Gundu Rao:** Conceptualization, Visualization, Investigation. **Alberto A. Ccollque-Quispe:** Writing – review & editing, Formal analysis. **Jorge Ayala-Arenas:** Investigation, Validation. **Monise B. Gomes:** Methodology, Software, Data curation. **Betzabel N. Silva-Carrera:** Methodology, Data curation. **Roseli F. Gennari:** Methodology, Investigation. **Valeria S. Pachas:** Methodology, Validation. **F. Monzon-Macedo:** Methodology, Software. **H. Loro:** Software, Data curation. **Jose F.D. Chubaci:** Supervision, Visualization. **Nilo F. Cano:** Writing – review & editing, Visualization. **René R. Rocca:** Methodology, Software, Data curation. **Shigueo Watanabe:** Supervision, Project administration, Funding acquisition.

Declaration of Competing Interest

The authors declare that they have no known competing financial interests or personal relationships that could have appeared to influence the work reported in this paper.

Data availability

Data will be made available on request.

Acknowledgment

The authors kindly acknowledge the financial support from CONCYTEC-PROCIENCIA, Peru, in the framework of the call E067-2022-04 (agreement no. PE501080404-2022-PROCIENCIA). In addition, the authors wish to thank Ms. E. Somessari from the Institute for Energy and Nuclear Researches (IPEN), Brazil, and Dr. H. Khoury from the Nuclear Energy Department of the Federal University of Pernambuco, Brazil, for kindly carrying out the irradiation of the samples.

References

[1] A. Miller, Techniques for high dose dosimetry in industry, agriculture and medicine, in: IAEA-TECDOC-1070, Proceedings of a Symposium, Vienna, Vienna 3, International Atomic Energy Agency, 2000, p. 305.

[2] J. Yang, L. Yang, W. Liu, Y. Zhang, H. Fan, Y. Wang, H. Liu, J. Lang, D. Wang, Luminescence behavior of Eu^{3+} in $CaSiO_3$:Eu^{3+}(Bi^{3+}) and Sr_2SiO_4:Eu^{3+}(Bi^{3+}), J. Alloys Compd. 454 (2008) 506–509, https://doi.org/10.1016/j.jallcom.2007.02.079.

[3] L. Zhou, B. Yan, Sol–gel synthesis and photoluminescence of $CaSiO_3$:Eu^{3+} nanophosphors using novel silicate sources, J. Phys. Chem. Solids 69 (2008) 2877–2882, https://doi.org/10.1016/j.jpcs.2008.07.012.

[4] Ž. Andrić, R. Krsmanović, M. Marinović-Cincović, T. Dramićanin, B. Šećerov, M. D. Dramićanin, Investigation on the crystallization process of Eu^{3+}: $CaSiO_3$ gel using optical and thermal methods, Acta Phys. Polonica A 112 (2007) 969–974, https://doi.org/10.12693/APhysPolA.112.969.

[5] S.C. Aynaya-Cahui, N.F. Cano, A.H. Lopez-Gonzales, T.K. Gundu Rao, M.B. Gomes, R.R. Rocca, J.F.D. Chubaci, S. Watanabe, J.S. Ayala-Arenas, Thermoluminescence and electron paramagnetic resonance correlation studies in lithium silicate phosphor, Solid State Sci. 123 (2022), 106777, https://doi.org/10.1016/j.solidstatesciences.2021.106777.

[6] C.D. Gonzales-Lorenzo, D.V. Ananchenko, S.V. Nikiforov, A.N. Kiryakov, A. F. Zatsepin, J.F.D. Chubaci, N.F. Cano, J.S. Ayala-Arenas, S. Watanabe, Effect of 130 keV pulsed electron irradiation on the efficiency of radiative transitions in Eu-doped glass-ceramics $CaSiO_3$, Opt. Mater. 119 (2021), 111304, https://doi.org/10.1016/j.optmat.2021.111304.

[7] C.D. Gonzales-Lorenzo, L.F. Nascimento, S. Kodaira, M.B. Gomes, S. Watanabe, Thermoluminescence studies of polycrystalline $CaSiO_3$ pellets for photons and particle therapy beams, Radiat. Phys. Chem. 177 (2020), 109132, https://doi.org/10.1016/j.radphyschem.2020.109132.

[8] C.D. Gonzales-Lorenzo, T.K.G. Rao, N.F. Cano, B.N. Silva-Carrera, R.R. Rocca, E. E. Cuevas-Arizaca, J.S. Ayala-Arenas, S. Watanabe, Thermoluminescence and defect centers in β-$CaSiO_3$ polycrystal, J. Lumin. 217 (2020), 116783, https://doi.org/10.1016/j.jlumin.2019.116783.

[9] C.D. Gonzales-Lorenzo, S. Watanabe, N.F. Cano, J.S. Ayala-Arenas, C.C. Bueno, Synthetic polycrystals of $CaSiO_3$ un-doped and Cd, B, Dy, Eu-doped for gamma and neutron detection, J. Lumin. 201 (2018) 5–10, https://doi.org/10.1016/j.jlumin.2018.04.037.

[10] S. Watanabe, N.F. Cano, L.S. Carmo, R.F. Barbosa, J.F.D. Chubaci, High- and very-high-dose dosimetry using silicate minerals, Radiat. Meas. 72 (2015) 66–69, https://doi.org/10.1016/j.radmeas.2014.11.004.

[11] M.R. Abass, H.M. Diab, M.M. Abou-Mesalam, New improved thermoluminescence magnesium silicate material for clinical dosimetry, Silicon 14 (2022) 2555–2563, https://doi.org/10.1007/s12633-021-01049-9.

[12] S. Katyayan, S. Agrawal, $CaSiO_3$: Eu^{2+}, Er^{3+}, $BaSiO_3$: Eu^{2+}, Er^{3+} and $SrSiO_3$: Eu^{2+}, Er^{3+} phosphors: molten salt synthesis, optical and thermal studies, J. Mater. Sci. 31 (2020) 8472–8480, https://doi.org/10.1007/s10854-020-03382-y.

[13] C.D. Gonzales-Lorenzo, S. Watanabe, T.A. Cavalieri, N.F. Cano, T.G. Rao, J. F. Chubaci, L.S. Carmo, C.C. Bueno, Calculated and experimental response of calcium silicate polycrystalline to high and very-high neutron doses, Radiat. Phys. Chem. 172 (2020), 108820, https://doi.org/10.1016/j.radphyschem.2020.108820.

[14] S.W.S. McKeever, Thermoluminescence of Solids, Cambridge University Press, 1985.

[15] E.G. Yukihara, S.W. McKeever, Optically Stimulated Luminescence: Fundamentals and Applications, John Wiley & Sons, 2011, https://doi.org/10.1002/9780470977064.

[16] M. Ikeya, New applications of electron spin resonance, 1993. https://doi.org/10.1142/1854.

[17] J.C. Mittani, M. Prokić, E.G. Yukihara, Optically stimulated luminescence and thermoluminescence of terbium-activated silicates and aluminates, Radiat. Meas. 43 (2008) 323–326, https://doi.org/10.1016/j.radmeas.2007.10.004.

[18] H. Nagabhushana, B.M. Nagabhushana, M. Madesh Kumar, Chikkahanumantharayappa, K.V.R. Murthy, C. Shivakumara, R.P.S. Chakradhar, Synthesis, characterization and photoluminescence properties of $CaSiO_3$:Eu^{3+} red phosphor, Spectrochim. Acta Part A 78 (2011) 64–69, https://doi.org/10.1016/j.saa.2010.08.063.

[19] R. Naik, S.C. Prashantha, H. Nagabhushana, S.C. Sharma, B.M. Nagabhushana, H. P. Nagaswarupa, H.B. Premkumar, Low temperature synthesis and photoluminescence properties of red emitting Mg_2SiO_4: Eu^{3+} nanophosphor for near UV light emitting diodes, Sens. Actuators B 195 (2014) 140–149, https://doi.org/10.1016/j.snb.2014.01.018.

[20] M.O. Onani, F.B. Dejene, Photo-luminescent properties of a green or red emitting Tb^{3+} or Eu^{3+} doped calcium magnesium silicate phosphors, Physica B 439 (2014) 137–140, https://doi.org/10.1016/j.physb.2013.11.003.

[21] G.R. Revannasiddappa, M.S. Rudresha, H. Nagabhushana, Combustion synthesis of $MgSiO_3$: Eu^{3+} (1–11 mol.%) nanophosphor: detection of eccrine latent fingerprints and anti-counterfeiting applications, Mater. Today 5 (2018) 22473–22480, https://doi.org/10.1016/j.matpr.2018.06.618.

[22] M. Somani, M. Saleem, M. Mittal, P.K. Sharma, Thermoluminescence studies of Ce^{3+} doped Sr_2SiO_4 phosphor, AIP Conf. Proc. 2100 (2019), 020157, https://doi.org/10.1063/1.5098711.

[23] N.M. Son, D.T. Tien, N.T.Q. Lien, V.X. Quang, N.N. Trac, T.T. Hong, H.V. Tuyen, Luminescence and thermal-quenching properties of red-emitting $Ca_2Al_2SiO_7$:Sm^{3+} phosphors, J. Electron. Mater 49 (2020) 3701–3707, https://doi.org/10.1007/s11664-020-08086-x.

[24] C. Zhu, S. Chaussedent, S. Liu, Y. Zhang, A. Monteil, N. Gaumer, Y. Yue, Composition dependence of luminescence of Eu and Eu/Tb doped silicate glasses for LED applications, J. Alloys Compd. 555 (2013) 232–236, https://doi.org/10.1016/j.jallcom.2012.12.052.

[25] S. Dhoble, N. Dhoble, R..B. Pode, Preparation and characterization of Eu^{3+} activated $CaSiO_3$, (CaA) SiO_3 [A = Ba or Sr] phosphors, Bull. Mater. Sci. 26 (2003) 377–382, https://doi.org/10.1007/BF02711179.

[26] M.M. Kumar, R.H. Krishna, B. Nagabhushana, C. Shivakumara, Synthesis, characterization and photoluminescence properties of Bi^{3+} co-doped $CaSiO_3$: Eu^{3+} nanophosphor, Spectrochim. Acta Part A 139 (2015) 124–129, https://doi.org/10.1016/j.saa.2014.11.095.

[27] D.V. Sunitha, H. Nagabhushana, F. Singh, B.M. Nagabhushana, S.C. Sharma, R.P. S. Chakradhar, Thermo, Iono and photoluminescence properties of 100 MeV Si^{7+} ions bombarded $CaSiO_3$:Eu^{3+} nanophosphor, J. Lumin. 132 (2012) 2065–2071, https://doi.org/10.1016/j.jlumin.2012.03.019.

[28] T. Gupta, Radiation, Ionization, and Detection in Nuclear Medicine, Springer, 2013, https://doi.org/10.1007/978-3-642-34076-5.

[29] M. Korzhik, G. Tamulaitis, A.N. Vasil'ev, Physics of Fast Processes in Scintillators, Springer, 2020, https://doi.org/10.1007/978-3-030-21966-6.

[30] W. Dai, Y. Lei, T. Yu, M. Peng, Q.Y. Zhang, Luminescence properties and a substitution defect model for self-reduction of europium ions in silicate Ba (Eu) $MgSiO_4$ phosphors, Mater. Res. Bull. 67 (2015) 176–184, https://doi.org/10.1016/j.materresbull.2015.03.004.

[31] S. Katyayan, S. Agrawal, Thermoluminescent behavior of UV and γ rays irradiated Eu^{2+} and Er^{3+} doped silicate phosphors, Mater. Chem. Phys. 225 (2019) 384–392, https://doi.org/10.1016/j.matchemphys.2018.12.096.

[32] B.B. Niraula, C. Rizal, Photoluminescence property of Eu^{3+} doped $CaSiO_3$ nano-phosphor with controlled grain size, Colloids Interfaces (2018), https://doi.org/10.3390/colloids2040052.

[33] R. Barve, B. Panigrahi, N. Suriyamurthy, B. Venkatraman, Luminescent properties of $CaSiO_3$: Ce^{3+}: a preliminary study, Physica B 612 (2021), 412925, https://doi.org/10.1016/j.physb.2021.412925.

[34] R. Dhanu, D. Prakashbabu, P. Bindu, M.M. Kumar, S. Ponkumar, R.H. Krishna, K. M. Rahulan, Photoluminescence of mixed phase $CaSiO_3$: Ce^{3+} nanophosphors, Optik 218 (2020), 165139, https://doi.org/10.1016/j.ijleo.2020.165139.

[35] C. Palan, K. Koparkar, N. Bajaj, S.K. Omanwar, Synthesis and TL/OSL properties of $CaSiO_3$: Ce biomaterial, Mater. Lett. 175 (2016) 288–290, https://doi.org/10.1016/j.matlet.2016.04.006.

[36] T. Yamanaka, H. Mori, The structure and polytypes of α-$CaSiO_3$ (pseudowollastonite), Acta Cryst. 37 (1981) 1010–1017, https://doi.org/10.1107/S0567740881004962.

[37] Y.V. Seryotkin, E.V. Sokol, S.N. Kokh, Natural pseudowollastonite: crystal structure, associated minerals, and geological context, Lithos 134 (2012) 75–90, https://doi.org/10.1016/j.lithos.2011.12.010.

[38] S.A. Speakman, Introduction to PANalytical X'Pert HighScore Plus v3. 0, MIT Center for Materials Science and Engineering, 2012, pp. 1–19.

[39] S.W.S. McKeever, On the analysis of complex thermoluminescence. Glow-curves: resolution into individual peaks, Phys. Status Solidi (a) 62 (1980) 331–340, https://doi.org/10.1515/9783112501528-040.

[40] P. Kivits, H.J.L. Hagebeuk, Evaluation of the model for thermally stimulated luminescence and conductivity; reliability of trap depth determinations, J. Lumin. 15 (1977) 1–27, https://doi.org/10.1016/0022-2313(77)90002-3.

[41] R. Chen, S.W.S. McKeever, Theory of Thermoluminescence and Related Phenomena, World Scientific, 1997, https://doi.org/10.1142/2781.

[42] G. Kitis, J.M. Gomez-Ros, J.W.N. Tuyn, Thermoluminescence glow-curve deconvolution functions for first, second and general orders of kinetics, J. Phys. D 31 (1998) 2636, https://doi.org/10.1088/0022-3727/31/19/037.

[43] H.G. Balian, N.W. Eddy, Figure-of-merit (FOM), an improved criterion over the normalized chi-squared test for assessing goodness-of-fit of gamma-ray spectral peaks, Nucl. Instrum. Methods 145 (1977) 389–395, https://doi.org/10.1016/0029-554X(77)90437-2.

[44] K.-W. Huang, W.-T. Chen, C.-I. Chu, S.-F. Hu, H.-S. Sheu, B.-M. Cheng, J.-M. Chen, R.-S. Liu, Controlling the activator site to tune europium valence in oxyfluoride phosphors, Chem. Mater. 24 (2012) 2220–2227, https://doi.org/10.1021/cm3011327.

[45] E. Malchukova, B. Boizot, Reduction of Eu^{3+} to Eu^{2+} in aluminoborosilicate glasses under ionizing radiation, Mater. Res. Bull. 45 (2010) 1299–1303, https://doi.org/10.1016/j.materresbull.2010.04.027.

[46] J.L. Merz, P.S. Pershan, Charge conversion of irradiated rare-earth ions in calcium fluoride. I, Phys. Rev. 162 (1967) 217–235, https://doi.org/10.1103/PhysRev.162.217.

[47] K.S.V. Nambi, V.N. Bapat, A.K. Ganguly, Thermoluminescence of $CaSO_4$ doped with rare earths, J. Phys. C 7 (1974) 4403, https://doi.org/10.1088/0022-3719/7/23/027.
[48] K.F. Hesse, Refinement of the crystal structure of wollastonite-2M (parawollastonite), Z. Krist. – Cryst. Mater. 168 (1984) 93–98, https://doi.org/10.1524/zkri.1984.168.14.93.
[49] R.D. Shannon, Revised effective ionic radii and systematic studies of interatomic distances in halides and chalcogenides, Acta Cryst. 32 (1976) 751–767, https://doi.org/10.1107/s0567739476001551.
[50] A. Herve, B. Maffeo, EPR identification of V1 centers in irradiated BeO, Phys. Lett. A 32 (1970) 247–248, https://doi.org/10.1016/0375-9601(70)90304-X.
[51] A. Herve, Doctoral Thesis, Grenoble University 1969.
[52] W. Williamson, J. Lunsford, C. Naccache, The EPR spectrum of O^- on magnesium oxide, Chem. Phys. Lett. 9 (1971) 33–34, https://doi.org/10.1016/0009-2614(71)80174-4.
[53] S. Misra, S. Andronenko, D. Tipikin, J. Freed, V. Somani, O. Prakash, Study of paramagnetic defect centers in as-grown and annealed TiO_2 anatase and rutile nanoparticles by a variable-temperature X-band and high-frequency (236 GHz) EPR, J. Magn. Magn. Mater. 401 (2016) 495–505, https://doi.org/10.1016/j.jmmm.2015.10.072.
[54] A. Ibarra, F. Lopez, M.J. de Castro, V centers in $MgAl_2O_4$ spinels, Phys. Rev. B 44 (1991) 7256, https://doi.org/10.1103/PhysRevB.44.7256.
[55] C.A. Hutchison Jr., Paramagnetic resonance absorption in crystals colored by irradiation, Phys. Rev. 75 (1949) 1769, https://doi.org/10.1103/PhysRev.75.1769.2.
[56] J.E. Wertz, P. Auzins, R. Weeks, R.J. Silsbee, Electron spin resonance of F centers in magnesium oxide; confirmation of the spin of magnesium-25, Phys. Rev. 107 (1957) 1535, https://doi.org/10.1103/PhysRev.107.1535.
[57] W.C. Holton, H. Blum, Paramagnetic resonance of F centers in alkali halides, Phys. Rev. 125 (1962) 89, https://doi.org/10.1103/PhysRev.125.89.